Nonlinear Hierarchical Easy-to-Implement Control for DC MicroGrids

Sabah B Siad, Alessio Iovine, Gilney Damm, Lilia Galai Dol, Mariana Netto

MDPI

Article

Nonlinear Hierarchical Easy-to-Implement Control for DC MicroGrids

Sabah B. Siad [1], Alessio Iovine [2],Gilney Damm [3]*, Lilia Galai-Dol [4], and Mariana Netto [5]

[1] L2S - Paris-Saclay University, Paris, France; sabah.siad-benamane@centralesupelec.f
[2] CNRS and L2S, CentraleSupélec, Université Paris-Saclay, 3, rue Joliot-Curie, 91192 Gif-sur-Yvette, France; alessio.iovine@centralesupelec.fr
[3] COSYS-LISIS, Univ. Gustave Eiffel, IFSTTAR, F-77447 Marne-la-Vallée, and with Efficacity Institute, Champs-sur-Marne, France; gilney.damm@univ-eiffel.fr
[4] CSTB, Champs-sur-Marne, France;Lilia.GALAIDOL@cstb.fr
[5] COSYS-PICSL, Univ. Gustave Eiffel, IFSTTAR, F-78000 Versailles, France; mariana.netto@univ-eiffel.fr
* Correspondence: gilney.damm@univ-eiffel.fr

Abstract: It was considered in this work the connection of a photovoltaics (PV) solar plant to the main grid through a Direct Current (DC) MicroGrid and a hybrid storage system, composed of a battery and a supercapacitor, in order to satisfy constraints of grid connection (the so-called Grid-Codes). The objective, and main contribution of this paper, is to stabilize the DC MicroGrid voltage in spite of large variations in production and consumption, using a nonlinear hierarchical easy-to-implement control strategy. Here it is presented the MicroGrid's control design based on detailed models of the photovoltaic energy sources and the storage systems. Such DC grids may present an unstable behavior created by the PV's intermittent output power, by switching ripples from the power converters and their power electronics, and oscillatory currents produced by some types of loads. Therefore the system is subject to both fast and slow variations, and its stabilization is based on different technologies of storage, such as battery and supercapacitor, and control algorithms designed thanks to the use of time-scale separation between different components of the storage systems. The obtained nonlinear results are stronger than current linear controllers, allowing to keep operating margins around the voltage reference. At the same time in this work, insights from power systems practice have been used, aiming to obtain a very simple and easy-to-implement control scheme. Detailed simulation results are provided to illustrate the behavior and effectiveness of the proposed stabilization technique.

Keywords: Microgrids; Power System Stability; Nonlinear control systems; Lyapunov methods; Power generation control

Citation: Siad, S.B.; Iovine, A.; Damm, G.; Galai-Dol, L.; Netto, M. Nonlinear Hierarchical Easy-to-Implement Control for DC MicroGrids. *Journal Not Specified* **2021**, *1*, 0. https://doi.org/

Received:
Accepted:
Published:

The integration of renewable energy sources (renewables) and modern loads on a large scale is a challenging task due to their intermittent nature. As a consequence, the power grid becomes vulnerable and subject to instability issues. In particular, the presence of Distributed Generation (DG) such as solar energy, or modern loads as electric vehicles and intelligent buildings in a distribution network creates challenges that can be addressed by the concept of MicroGrids [1], [2]. In MicroGrids, storage devices are used to compensate for intermittent behavior and then secure grid integrity concerning the increase in the number of DG elements [3]. They allow for the possibility to design control systems to ensure stability during the injection and consumption of intermittent power.

The present paper focuses on stabilizing voltage on a Direct Current (DC) MicroGrid, used to integrate renewable power. This stabilization is obtained by designing a hierarchical control strategy that considers the power balance between the energy sources and loads. The nonlinear control scheme has been developed for a DC MicroGrid composed of photovoltaic (PV) panels, two storage devices (a battery and a supercapacitor)

acting at different time scales, a DC load and its connection to an Alternate Current (AC) grid.

In the field of MicroGrids, linear control methods are generally used, as in [4], [5], [6], [7] and [8]. These works use the small signal model of converters, and apply the industrial standard PI control, mostly addressing the stabilisation of the MicroGrid's DC voltage. On those workd, the control voltage performances are acceptable in terms of voltage overshoot and settling time, and stabilization of the whole DC MicroGrid is attained. Nevertheless, such control methods can correctly stabilize a MicroGrid only in steady state, when parameters do not vary much. On the other hand, if several parameters are time-varying, such linear controllers can not ensure good performance (sometimes not even stability) for the several operating points associated with such variations. Therefore, developing new control structures to improve systems' performance is necessary.

On another hand, ([9],[10], [11]) propose new control strategies based on nonlinear control theory, using state average model of converters. On those, the control strategy is designed globally with high level controller, and act locally on converters with local control algorithm. With this control strategy the system should be able to balance supply power and demand load in order to obtain a good performance in transient conditions and steady-state. Nevertheless, such results are rather complex, with algorithms that are difficult to implement in small and low-cost micro-controllers, distributed on a large number of components. The now proposed control philosophy is also based on a Systems of Systems approach, where each brick is designed to participate in ensuring the stability of the whole DC voltage system. This control strategy was developed in ([12], [13], [14], [15], [16], [17]), addressing different applications. In the present paper, such techniques were used to design a control strategy to stabilize the DC MicroGrid voltage through a control algorithm that defines priorities in relation to the photovoltaic system, load, and constraints for storage system operation.

Other articles (see [18], [19], [20], [21]) have also proposed a hierarchical control scheme focusing on a centralized supervisory control level and a distributed lower level control, based on nonlinear theory. These controllers present rigorous analysis of the interaction between the different dynamics, and aim to stabilize the whole system, even when large variations of power production and consumption occur, and to ensure power quality while providing power to the main AC grid. Differently to those results, the present paper has used assumptions coming from the physics of power systems to reduce the complexity of the control design procedure. However, these assumptions make stability analysis to hold inside a smaller operation region than more complex results. Nevertheless, these insights from power systems' practice allow simpler algorithms, well suited for a distributed implementation in low-cost micro-controllers in a low voltage grid, and still allow to stand large disturbances inside a well-defined operation region.

In this scheme, the higher-level controller provides reference values for the local controllers. Thereafter, we develop these distributed controllers using backstepping, feedback linearization, and Lyapunov-based control techniques. Power system stability is analyzed by intermediate Lyapunov functions provided for each step to construct a composite Lyapunov function for the overall stability analysis. The local controllers are implemented at the actuators' level on each device's power converters (PV panel, battery, supercapacitor). The reference is obtained by a Maximum Power Point Tracking (MPPT) algorithm concerning the PV power source. The supervisory higher-level controller is allowed to reduce the power reference in case of overproduction. The higher-level controller provides power references for the storage devices to cope with power unbalance in the whole system.

This paper is organized as follows. In Section I, the model for the DC MicroGrid is introduced; in Section II the DC MicroGrid Control strategy is drawn; in Section III low level control laws for each subsystem are designed; in Section IV the stability analysis for

the overall interconnected system is done; Section V provides simulation results about the connected system behavior; finally, Section VI presents the conclusions.

1. DC Microgrid Model

A general DC MicroGrid as in Figure 1 is composed of Distributed Generation (DG) such as photovoltaic arrays, energy storage elements like supercapacitors and batteries, DC loads and grid-tied converters [22]. The energy storage elements play an important role for the entire power management of the DC MicroGrid as mentioned. They ensure a secured network, provide high quality power and maintain the common DC grid voltage stable [23]. Bidirectional converters are used to charge or discharge the energy storage elements such as the battery and the supercapacitor. The load (an electric vehicle charge station for example) is modelled as a variable resistance, which in the present case are more delicate than constant power loads.

In the following, the different components of the DC MicroGrid are described.

1.1. PV System Modeling

1.1.1. Solar Array

A complete solar panel model with series and parallel connection is proposed [24],[25]. The PV is represented as a current source. Due to the variations of the temperature and the solar radiance, the current and the voltage generated by the PV panel vary.

The PV DC/DC boost converter operates following references given by a standard MPPT algorithm (not discussed in this paper) under varying levels of irradiation and temperature [25],[26] and [24].

1.1.2. DC/DC Boost Converter

The DC/DC converter used to control the PV array is an unidirectional boost converter. It is represented by three state variables: the voltages on the capacitors C_1 and C_2 and the current in the inductance L_1.

The mathematical model for the DC/DC boost converter that interconnects the PV to the DC grid is obtained based on power electronics averaging technique (see [27], [28], [29], [30]), and is given by (1).

1.2. Storage system

The hybrid storage system (battery-supercapacitor) adopts the advantages of both technologies, high power density from the supercapacitor and high energy density from the battery. The proposed hybrid storage consists of a lead acid battery and a supercapacitor, as in [31], [32],[3] and [33].

1.2.1. Battery model

The chosen model for the study is based on the resistive Thevenin model for a Lead Acid Battery, considered as a voltage generator [34].

1.2.2. Supercapacitor

The Supercapacitor is modelled by the so-called three-branch model, extracted from the transmission line modelling. It is connected to the DC grid by a DC/DC bidirectional boost converter as in [35] and [36].

1.2.3. Bidirectional Boost Converters

The bidirectional boost converter controlling the battery is given by (2), based on the voltages on the capacitors C_3 and C_4 and the current in the inductance L_2 (see [37], [29,32] and [30]).

The bidirectional boost converter controlling the supercapacitor is modelled based on the voltages on the capacitors and the current in the inductance C_5, C_6, L_3, shown by (3), (see [29], [32] and [30]).

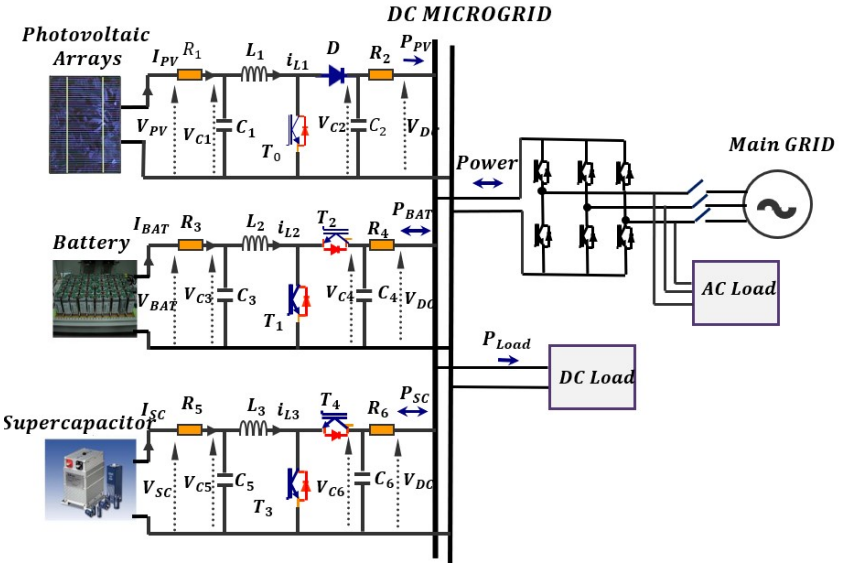

Figure 1. The considered DC MicroGrid.

1.3. Interconnected Model

The mathematical model for the DC grid in Figure 1 is obtained based on the power electronics averaging technique [27]:

$$\dot{V}_{C1} = -\frac{1}{R_1 C_1} V_{C1} - \frac{1}{C_1} i_{L1} + \frac{1}{R_1 C_1} V_{PV} \tag{1a}$$

$$\dot{V}_{C2} = -\frac{1}{R_2 C_2} V_{C2} + \frac{(1-u_1)}{C_2} i_{L1} + \frac{1}{R_2 C_2} V_{DC} \tag{1b}$$

$$\dot{i}_{L1} = \frac{1}{L_1} V_{C1} - \frac{(R_{01} - R_{02})u_1 + R_{02}}{L_1} i_{L1} - \frac{(1-u_1)}{L_1} V_{C2} \tag{1c}$$

$$\dot{V}_{C3} = -\frac{1}{R_3 C_3} V_{C3} - \frac{1}{C_3} i_{L2} + \frac{1}{R_3 C_3} V_{BAT} \tag{2a}$$

$$\dot{V}_{C4} = -\frac{1}{R_4 C_4} V_{C4} + \frac{(1-u_2)}{C_4} i_{L2} + \frac{1}{R_4 C_4} V_{DC} \tag{2b}$$

$$\dot{i}_{L2} = \frac{1}{L_2} V_{C3} - \frac{(R_{03} - R_{04})u_2 + R_{04}}{L_2} i_{L2} - \frac{(1-u_2)}{L_2} V_{C4} \tag{2c}$$

$$\dot{V}_{C5} = -\frac{1}{R_5 C_5} V_{C5} - \frac{1}{C_5} i_{L3} + \frac{1}{R_5 C_5} V_{SC} \tag{3a}$$

$$\dot{V}_{C6} = -\frac{1}{R_6 C_6} V_{C6} + \frac{(1-u_3)}{C_6} i_{L3} + \frac{1}{R_6 C_6} V_{DC} \tag{3b}$$

$$\dot{i}_{L3} = \frac{1}{L_3} V_{C5} - \frac{(R_{05} - R_{06})u_3 + R_{06}}{L_3} i_{L3} - \frac{(1-u_3)}{L_3} V_{C6} \tag{3c}$$

$$\dot{V}_{DC} = \frac{1}{C_{DC}} \left[\frac{1}{R_2} (V_{C2} - V_{DC}) + i_{L2} + i_{L3} - \frac{P_{load}}{V_{DC}} \right] \tag{4a}$$

where R_1, R_2, R_3, R_4, R_5, R_6, L_1, L_2, L_3, C_1, C_2, C_3, C_4, C_5, C_6 and C_{DC} are known positive values of resistances, inductances and capacitors respectively, and P_{load} represents the DC demanded power load. To model the switches, small resistances $(R_{01}, R_{02}, R_{03}, R_{04}, R_{05}$ and $R_{06})$ are included to take into account conduction losses. V_{PV}, V_{BAT}, V_{SC} and V_{DC} are the photovoltaic panel, battery, supercapacitor and DC MicroGrid voltages, respectively. The measured output vector is composed by $V_{C1}, V_{C2}, V_{C3}, V_{C4}, V_{C5}, V_{C6}, i_{L1}, i_{L2}, i_{L3}$ and V_{DC}. The control inputs u_1, u_2 and u_3 represent the duty cycles of each converter. Equation (4) describes by Kirchhoff's law the voltage variation due to the sum of all currents in the DC bus V_{DC}.

2. DC MicroGrid Control strategy

The target for the controller is to stabilize the DC bus voltage around the desired value, then ensuring power quality and allowing the DC MicroGrid to manage the desired amount of power. The proposed control will be based on two control layers (see Figure 2). First, we define the high level controller to give reference values for lower local controllers. Thereafter, we develop a local control using backstepping and Lyapunov based techniques.

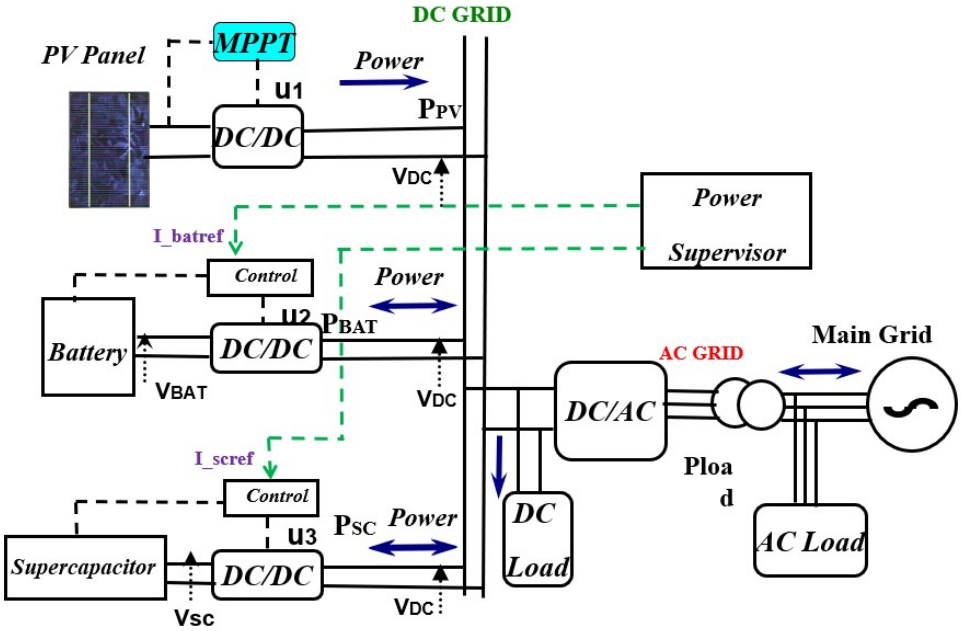

Figure 2. DC MicroGrid Control strategy.

2.1. High Level Controller for PV array source

A Maximum Power Point Tracking (MPPT) algorithm is used to extract the maximum power from a photovoltaic array of solar cells. To accomplish this task, a V_{C1}^* time varying (piecewise constant) desired voltage reference is provided by the MPPT. In this paper, the Incremental Conductance method is applied (see [25] , [38]and [39]).

2.2. High Level Controller for Storage system

We rely on the storage system (battery + supercapacitor) to act as a buffer to absorb the current (power) variations and stabilize the DC bus. Based on the physical characteristics of the storage components, and in particular on the current limitations from the battery, we indicate: 1- to consider a current reference i_{ST}^* based on power balance equations for the whole system; 2- to use a time-scale separation to decompose it in two components, a fast one (i_{L3}^*) and a slow one (i_{L2}^*), as shown in Figure 3. The slow component will be used as the reference for the battery's power supply, while the fast

component will be the reference power for the supercapacitor. This time scale separation is obtained by the introduction of a first order low pass filter that decomposes the current reference in two references for the battery and supercapacitor [40]

$$i_{ST}^{*} = i_{L2}^{*} + i_{L3}^{*} \tag{5}$$

The two components are chosen to keep sufficient time-scale separation between the lower and higher level control objectives (see [41]), and to ensure that the battery does not need to react faster than its specifications allow. Therefore, we target to extend the lifespan of the battery [10].

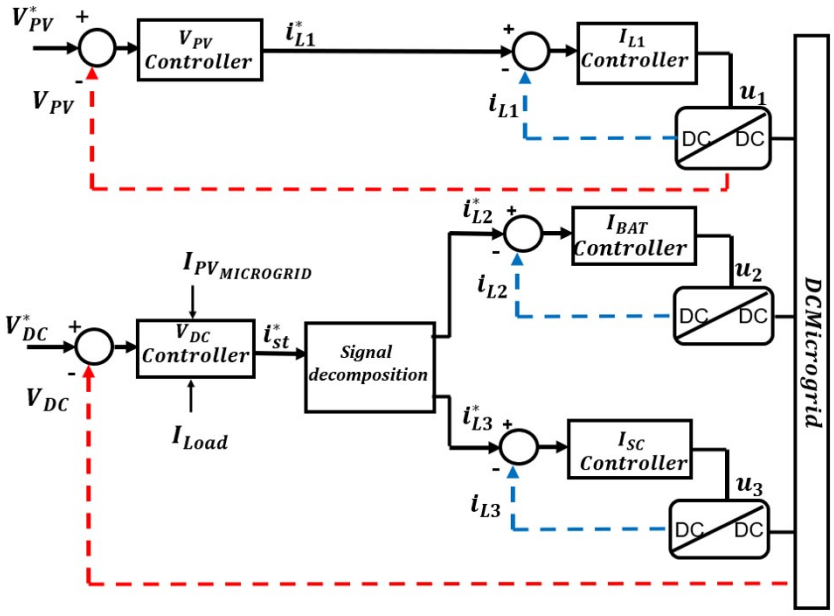

Figure 3. The adopted time-scale depending control strategy.

The power flow of the different elements of DC MicroGrid (see [22]) will depend on the grid topology. Most works consider a radial DC MicroGrid for its simplicity while yet capturing most challenges existing in DC MicroGrids. Radial systems are easier for installation and operation and meet the objective of designing a plug and play system which allows a larger penetration of renewable energy into the network. The proposed control strategy is also applicable for ring or bus [42] topologies (which are simpler than radial), and may also be implemented in meshed ones. For the latter it would be necessary to prevent congestion problems, that is not addressed in the present paper, and is usually dealt with higher-level controllers, closer to optimization and communication techniques. Bus topology is currently used in residential buildings, where low voltage DC bus is preferred to match the voltage level of many appliances and to avoid extra DC-DC conversion stages. Also in such systems, loads and AC grid interface can be located close to each other in order to reduce the distribution losses [43]. A radial grid is shown in Figure 4 while a ring DC MicroGrid is shown in Figure 5. The sum of the output power of all generating units (photovoltaic system in the present case), all loads and the storage system is defined as follows:

$$P_{DC} = P_{PV} + P_{Load} + P_{ST} \tag{6}$$

with $P_{ST} = P_{BAT} + P_{SC}$, where P_{PV} is the PV power, P_{ST} is the storage power, P_{BAT} is the battery power, P_{SC} is the supercapacitor power, P_{Load} is the load power and P_{DC} is the DC grid power.

In general, the DC MicroGrid is connected to the main AC Grid then $P_{DC} = P_{GRID}$, and the balance power is supplied to or obtained from the AC Grid (P_{GRID} being the

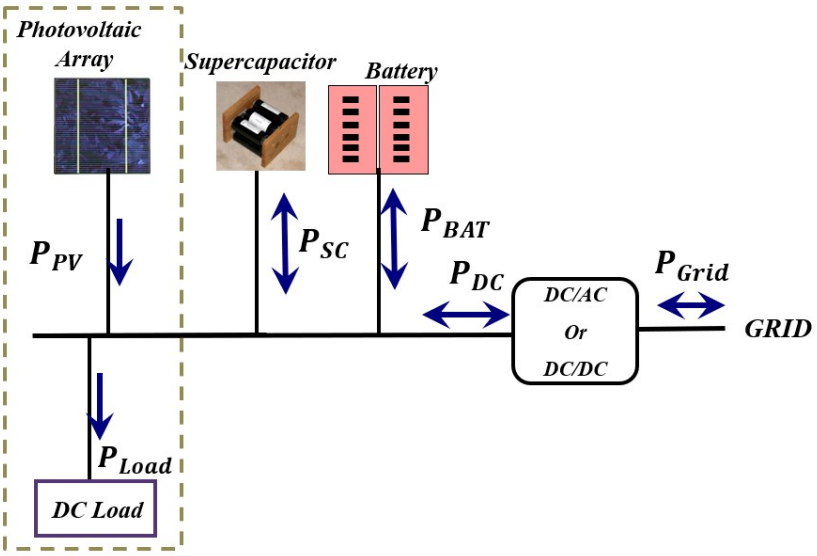

Figure 4. The Power Flow scheme.

power from or to the AC grid). In the present paper, we investigate the more difficult case corresponding to when the DC MicroGrid is in islanded mode, and we can not rely on the AC network to balance the DC grid. In this case, any unbalance on the power flow will create a voltage excursion on the DC grid.

The energy storage elements can switch between charge and discharge mode in order to maintain the DC grid power balance. $V_{DC}(t)$ must be kept around its nominal value V_{DC}^* and inside voltage limits following the power balance given by equation (4). It is possible to rewrite equation (4) as:

$$\dot{V}_{DC} = \frac{1}{C_{DC}}\left[\frac{1}{R_2}(V_{C2} - V_{DC}) + \frac{P_{ST} - P_{Load}}{V_{DC}}\right] \tag{7}$$

In the following, i_{ST}^* as in (5) is designed for i_{L2} and i_{L3}, in order to steer V_{DC} to its reference V_{DC}^* using backsteeping techniques [44]. Let us define the output tracking error $e_{V_{DC}} = (V_{DC} - V_{DC}^*)$. Based on the error dynamics, we suggest the following current reference:

$$\begin{aligned} i_{ST}^* \quad = \quad & \frac{P_{Load}}{V_{DC}} - \frac{1}{R_2}(V_{C2} - V_{DC}) \\ & -C_{DC}(K_{10}e_{V_{DC}} + \overline{K}_{10}\alpha_{10}) \end{aligned} \tag{8}$$

with:

$$\dot{\alpha}_{10} = K_{10}^{\alpha} e_{V_{DC}}$$

where α_{10} represents an integral error term, and K_{10}, $\overline{K}_{10}$ and K_{10}^{α} are positive tuning gain parameters.

Due to time-scale consideration between the voltage and current dynamics, in the sequel we consider V_{DC} as a zero dynamics of the system, so i_{ST} can be considered already equal to i_{ST}^*, such that inside an operation region ($\mathcal{D} = \{e_{V_{DC}} \in \mathbb{R} \mid e_{V_{DC}} \leq V_{DC_{Max}}\}$ for a desired constant $V_{DC_{Max}}$) and we can write:

$$\begin{bmatrix} \dot{\alpha}_{10} \\ \dot{e}_{V_{DC}} \end{bmatrix} = \begin{bmatrix} 0 & K_{10}^{\alpha} \\ -\overline{K}_{10} & -K_{10} \end{bmatrix} \begin{bmatrix} \alpha_{10} \\ e_{V_{DC}} \end{bmatrix}$$

As a consequence, the closed-loop dynamics of V_{DC} results to be linear and exponentially stable, with desired dynamics given by the stable poles assigned by the tuning

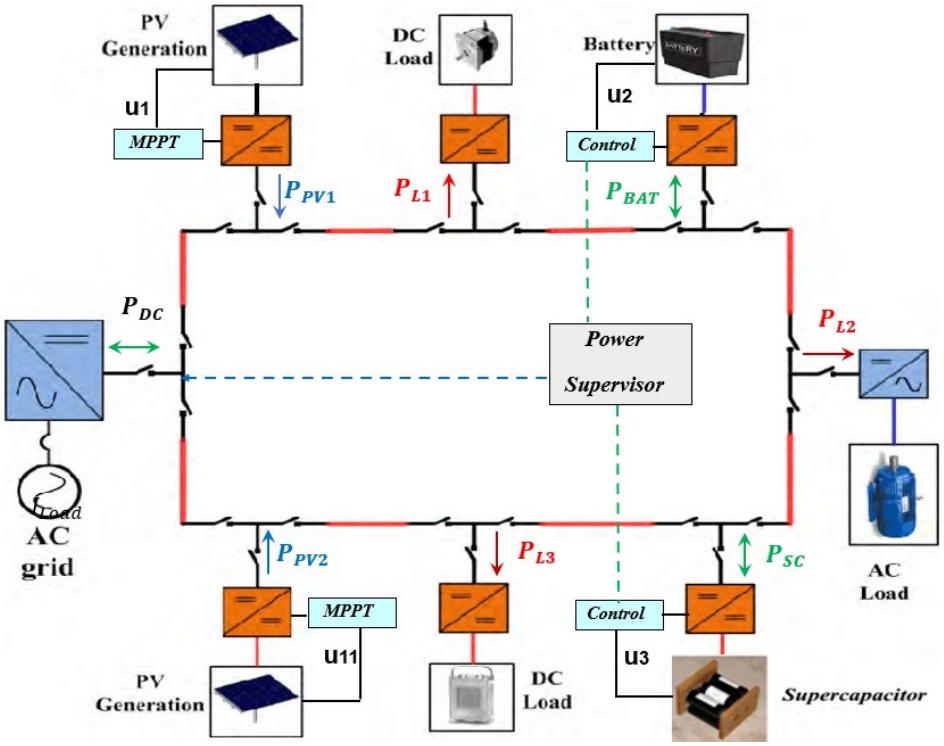

Figure 5. Ring DC MicroGrid Topology

gains. Then, there exists $P_{10} = P_{10}^T > 0$ such that $P_{10}A_{10} + A_{10}^T P_{10} = I_2$, where I_2 is the identity matrix in $\mathbb{R}^2$, such that the Lyapunov function:

$$W_{10} = [\alpha_{10}\ e_{V_{DC}}]^T\ P_{10}\ [\alpha_{10}\ e_{V_{DC}}] > 0 \tag{9}$$

exists, which time derivative is negative definite:

$$\dot{W}_{10} = -e_{V_{DC}}^2 - \alpha_{10}^2 < 0. \tag{10}$$

3. Local Control Level

3.1. Storage System Control

3.1.1. Battery Control Law

Taking the i_{L2}^* reference value for i_{L2}, it is possible to compute the control law by feedback linearization. First, we define the output tracking error:

$$e_{i_{L2}} = (i_{L2} - i_{L2}^*)$$

and consider the control law [11]:

$$\begin{aligned} u_2 = & \frac{1}{(V_{C4} + (R_{04} - R_{03})i_{L2})}[-(V_{C3} - V_{C4}) + R_{04}i_{L2} \\ & -L_2(K_6(i_{L2} - i_{L2}^*) + \overline{K}_6\alpha_6) + \dot{i}_{L2}^*] \end{aligned} \tag{11}$$

where $\dot{i}_{L2}^*$ is obtained through a derivative filter, α_6 represents an integral term and K_6, $\overline{K}_6$ and K_6^α are the positive tuning gain parameters. By technological reasons, the following condition is always fulfilled:

$$V_{C4} + (R_{04} - R_{03})i_{L2} \neq 0. \tag{12}$$

Consequently, the closed loop system is shown to be linear and exponentially stable [11]:

$$\begin{aligned} \dot{\alpha}_6 &= K_6^{\alpha} e_{i_{L2}} \\ \dot{e}_{i_{L2}} &= -K_6 e_{i_{L2}} - \overline{K_6}\alpha_6 \end{aligned} \tag{13}$$

3.1.2. Supercapacitor Control Law

We define the output tracking error $e_{i_{L3}} = (i_{L3} - i_{L3}^*)$ and its derivative $\dot{e}_{i_{L3}} = (\dot{i}_{L3} - \dot{i}_{L3}^*)$.

As in the previous case, we consider a control law u_3 by input/output feedback linearization such as to steer i_{L3} towards its reference i_{L3}^*, imposing the desired dynamic closed-loop behaviour, where α_9 represents an integral error term and K_9, $\overline{K}_9$ and K_9^{α} are the positive tuning gain parameters:

$$\begin{aligned} u_3 &= \frac{1}{(V_{C6} + (R_{06} - R_{05})i_{L3}}[-V_{C5} + V_{C6} + R_{05} i_{L3} \\ &\quad -L_3(K_9(i_{L3} - i_{L3}^*) + \overline{K}_9\alpha_9 + \dot{i}_{L3}^*)] \end{aligned} \tag{14}$$

Consequently, the closed loop system results linear and exponentially stable [11]:

$$\begin{aligned} \dot{\alpha}_9 &= K_9^{\alpha} e_{i_{L3}} \\ \dot{e}_{i_{L3}} &= -K_9 e_{i_{L3}} - \overline{K_9}\alpha_9 \end{aligned} \tag{15}$$

We remark that $\dot{i}_{L3}^*$ is obtained as $\dot{i}_{L2}^*$ in (11), and we need to consider a condition similar to the one in with (12) (always fulfilled by technological reasons):

$$V_{C6} + (R_{06} - R_{05})i_{L3} \neq 0. \tag{16}$$

The control inputs u_2 and u_3 feedback linearize the dynamics of i_{L2} and i_{L3}. Because of the linearity of the stable closed loop system, there exist matrices $P_{6,9} = P_{6,9}^T > 0$ such that $P_{6,9}A_{6,9} + A_{6,9}^T P_{6,9} = -I_2$, where I_2 is an identity matrix in $\mathbb{R}^2$. Therefore, we introduce the candidate Lyapunov function:

$$W_{69} = [\alpha_6\ e_{i_{L2}}]^T\ P_6\ [\alpha_6\ e_{i_{L2}}] + [\alpha_9\ e_{i_{L3}}]^T\ P_9\ [\alpha_9\ e_{i_{L3}}] \tag{17}$$

which time derivative is:

$$\dot{W}_{69} = -e_{i_{L2}}^2 - \alpha_6^2 - e_{i_{L3}}^2 - \alpha_9^2 < 0. \tag{18}$$

3.2. PV System Control

Based on (1), the control target for the PV array is to stabilize the voltage capacitor V_{C1} around the time varying (piecewise constant) reference value V_{C1}^*, provided by the MPPT algorithm. Similarly to [10], we state the assumption that the current can be set to have much faster dynamics than the capacitances' voltages. This allows the current and voltage regulation to be in a cascaded control scheme, with an inner current loop and an outer voltage loop. Consequently, a reference i_{L1}^* for i_{L1} will be designed to steer V_{C1} to its reference V_{C1}^*. To this purpose, we define the tracking errors:

$$e_{V_{C1}} = (V_{C1} - V_{C1}^*) \text{ and } e_{i_{L1}} = (i_{L1} - i_{L1}^*).$$

Then, similarly to [11], we consider the tracking reference as:

$$i_{L1}^* = \frac{1}{R_1}(V_{PV} - V_{C1}) + C_1 K_1 (V_{C1} - V_{C1}^*) + C_1 \overline{K}_1^{\alpha}\alpha_1 \tag{19}$$

and the control law:

$$\begin{aligned} u_1 &= \frac{1}{V_{C2} + (R_{02} - R_{01})i_{L1}}[V_{C2} - V_{C1} \\ &+ R_{02} i_{L1} L_1 (K_3 e_{i_{L1}} + \overline{K}_3 \alpha_3) \\ &- C_1 \overline{K}_1 K_1^{\alpha} e_{V_{C1}} \\ &+ (C_1 K_1 - \frac{1}{R_1})(K_1 e_{V_{C1}} + \overline{K}_1 \alpha_1))\Big] \end{aligned} \tag{20}$$

where α_1 and α_3 represent the integral terms assuring zero error in steady state between the dynamics of the states and their references:

$$\dot{\alpha}_1 = K_1^{\alpha} e_{V_{C1}} \text{ and } \dot{\alpha}_3 = K_3^{\alpha} e_{i_{L1}}$$

and where K_1, $\overline{K}_1$, K_1^{α}, K_3, $\overline{K}_3$ and K_3^{α} are positive tuning gain parameters. As before, the control input u_1 feedback linearizes the dynamics of V_{C1} and i_{L1}, and the closed loop results to be linear and exponentially stable [11]:

$$\dot{e}_{V_{C1}} = -K_1 e_{V_{C1}} - \overline{K_1}\alpha_1 \tag{21}$$

$$\dot{e}_{i_{L1}} = -K_3 e_{i_{L1}} - \overline{K_3}\alpha_3 \tag{22}$$

As a consequence, there exist matrices $P_{1,3} = P_{1,3}^T > 0$ such that $P_{1,3}A_{1,3} + A_{1,3}^T P_{1,3} = -I_2$, I_2 is an identity matrix in $\mathbb{R}^2$. Then, we introduce the Lyapunov function for the dynamics of V_{C1} and i_{L1} and its derivative as:

$$W_{13} = [\alpha_1 \; e_{V_{C1}}]^T \; P_1 \; [\alpha_1 \; e_{V_{C1}}] \; + \; [\alpha_3 \; e_{i_{L1}}]^T \; P_3 \; [\alpha_3 \; e_{i_{L1}}] \tag{23}$$

$$\dot{W}_{13} = -e_{V_{C1}}^2 - \alpha_1^2 - e_{i_{L1}}^2 - \alpha_3^2 < 0. \tag{24}$$

4. Stability study of the interconnected system

It is possible to split the states into controlled variables V_{C1}, i_{L1}, i_{L2}, i_{L3} and V_{DC} and the zero dynamics (uncontrolled variables) V_{C2}, V_{C3}, V_{C4}, V_{C5} and V_{C6}. With respect to the equilibrium points given by the references, the calculation of the missing equilibrium points V_{C2}^e, V_{C3}^e, V_{C4}^e, V_{C5}^e and V_{C6}^e can be easily done by steady-state considerations for the closed loop system.

Lemma 4.1. *Under the assumption that for each time the conditions:* $V_{C2} + (R_{02} - R_{01})i_{L1} \neq 0$, $V_{C4} + (R_{04} - R_{03})i_{L2} \neq 0$ *and* $V_{C6} + (R_{06} - R_{05})i_{L3} \neq 0$, *there exist control laws* u_1, u_2 *and* u_3 *given by (20), (11) and (14) such that the system (1), (2), (3), (4), has in closed loop an equilibrium point* x_e *and any initial condition exponentially converges to it.*

Proof. The proof is based on a Lyapunov function W, which is a composition of the previous Lyapunov functions. We consider the closed loop system with respect to the control inputs u_1, u_2 and u_3 already defined for controlling the dynamics of V_{C1}, i_{L1}, i_{L2}, i_{L3} and V_{DC}. They were proven to be stable by the Lyapunov functions $W_{1.3}$, $W_{6.9}$ and W_{10}. These Lyapunov functions, provided for each step, will be used for the entire system by a composite Lyapunov function. The Lyapunov function V is then defined as:

$$W = W_{13} + W_{69} + W_{10} + W_{23456} \tag{25}$$

where W_{13}, W_{69} and W_{10} have already been introduced and W_{23456} refers to dynamics V_{C2}, V_{C3}, V_{C4}, V_{C5} and V_{C6}. We introduce the errors $e_{V_{C2}}$, $e_{V_{C3}}$, $e_{V_{C4}}$, $e_{V_{C5}}$ and $e_{V_{C6}}$ between

the remaining voltage dynamics and their equilibrium points, and consider a candidate Lyapunov function W_{23456} as:

$$W_{23456} = \frac{R_2C_2}{2}e_{V_{C2}}^2 + \frac{R_3C_3}{2}e_{V_{C3}}^2 + \frac{R_4C_4}{2}e_{V_{C4}}^2 + \frac{R_5C_5}{2}e_{V_{C5}}^2 + \frac{R_6C_6}{2}e_{V_{C6}}^2.$$

Its time derivative is:

$$\dot{W}_{23456} = -e_{V_{C2}}^2 - e_{V_{C3}}^2 - e_{V_{C4}}^2 - e_{V_{C5}}^2 - e_{V_{C6}}^2 < 0$$

Finally, we consider the composition of the Lyapunov functions for the whole system:

$$\begin{aligned} W_{1\cdots10} &= ([\alpha_1\ e_{V_{C1}}]^T\ P_1[\alpha_1 e_{V_{C1}}]) + ([\alpha_2 e_{i_{L1}}]^T P_2[\alpha_2 e_{i_{L1}}]) \\ &+ \frac{R_2C_2}{2}e_{V_{C2}}^2 + \frac{R_3C_3}{2}e_{V_{C3}}^2 + \frac{R_4C_4}{2}e_{V_{C4}}^2 \\ &+ ([\alpha_6\ e_{i_{L2}}]^T\ P_6\ [\alpha_6\ e_{i_{L2}}]) + \frac{R_5C_5}{2}e_{V_{C5}}^2 + \frac{R_6C_6}{2}e_{V_{C6}}^2 \\ &+ ([\alpha_9\ e_{i_{L3}}]^T\ P_9[\alpha_9 e_{i_{L3}}]) + ([\alpha_{10}\ e_{V_{DC}}]^T\ P_{10}[\alpha_{10}\ e_{V_{DC}}]) > 0 \end{aligned}$$

which time derivative is:

$$\begin{aligned} \dot{W}_{1\cdots10} &= -e_{V_{C1}}^2 - \alpha_1^2 - e_{i_{L1}}^2 - \alpha_2^2 - e_{V_{C2}}^2 \\ &- e_{V_{C3}}^2 - e_{V_{C4}}^2 - e_{i_{L2}}^2 - \alpha_6^2 - e_{V_{C5}}^2 - e_{V_{C6}}^2 - e_{i_{L3}}^2 \\ &- e_{V_{DC}}^2 - \alpha_9^2 - \alpha_{10}^2 < 0 \end{aligned}$$

Then, exponential convergence of all states of the interconnected system towards their equilibrium points is ensured. □

5. Simulation Results

In this section we present simulations using detailed switching models on Simscape Electrical from Matlab Simulink. These simulations allow to isolate the control and dynamic response phenomena, while still representative for the remaining power electronic aspects.

R_{01}	0.001Ω	R_1	0.1Ω	C_1	$0.1F$
R_{02}	0.002Ω	R_2	0.001Ω	C_2	$0.01F$
R_{03}	0.001Ω	R_3	0.5Ω	C_3	$0.1F$
R_{04}	0.0015Ω	R_4	0.01Ω	C_4	$0.01F$
R_{05}	0.001Ω	R_5	0.4Ω	C_5	$0.1F$
R_{06}	0.0015Ω	R_6	0.01Ω	C_6	$0.01F$
L_1	$0.0033H$	L_2	$0.0033H$	L_3	$0.0033H$
V_{PV}	$1000V$	P_n	$1MW$	V_{DC}	$1000V$
V_{SC}	$500V$	V_{BAT}	$500V$	V_{DC}	$1000V$

Table 1: Simulation parameters.

Two simulations are presented. The first one is done during 300s of simulation time, and aims to show the system power characteristics and energy behavior. The second is done during 50s of simulation time, and focuses on the dynamic performance of the proposed control.

Figure 6 in the left shows the output power for the photovoltaic system with varying irradiance. It can be seen that the output power follows the irradiance variations. Figure

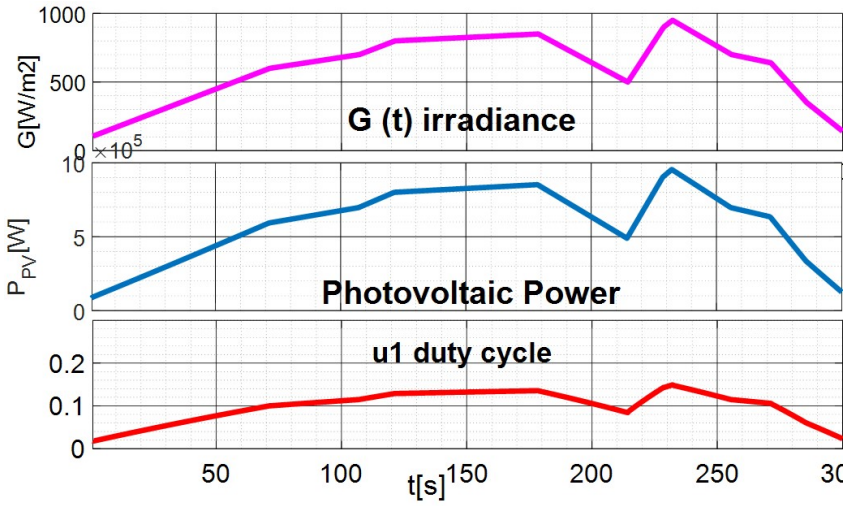

Figure 6. PV with Varying Irradiance.

6 in the right shows the control input u_1, which is bounded between zero and 1. One can see that the local controller keeps the PV tracking its Maximum Power Point.

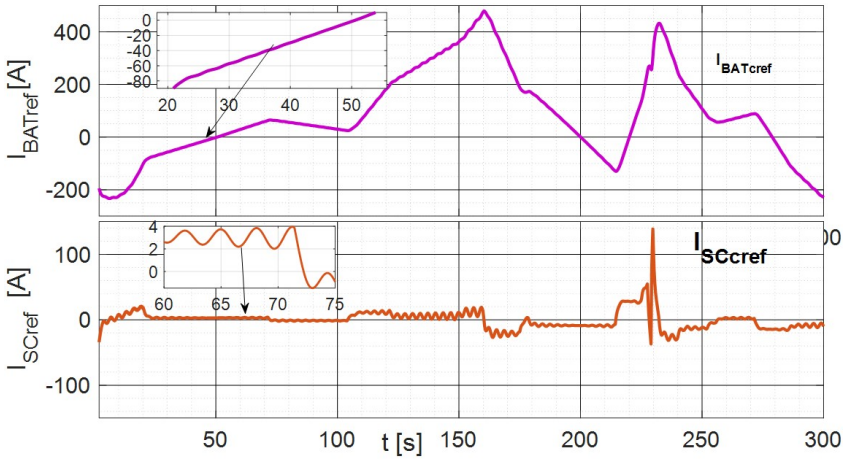

Figure 7. Power reference components (top graph: i^*_{L3}, bottom graph: i^*_{L2}).

Figure 7 shows the signal decomposition from equation (5), with fast and slow references shown in the top and the bottom figures respectively.

Figure 8 shows the control input u_2 which is bounded between zero and one and the output power from the battery.

Figure 9 shows the control inputs u_3, which are bounded between zero and one, and the output power from the supercapacitor. The Figures 8 and 9 show the control inputs are smooth except in the case of fast power variations of different elements of the DC MicroGrid. Concerning the output power from the battery and the supercapacitor, fast time-varying signals are instantaneously absorbed by the supercapacitor P_{SC}, such that the battery can remain rather unchanged during fast perturbations. This is capital to ensure a long lifespan for the battery. This one can then provide most of the energy demanded by the load, allowing long term stability and the use of weather forecast and load predictions in the higher level algorithms.

Figure 10 shows the output power for different elements of the DC MicroGrid. We can remark that the variation of storage power follows the variation on PV and load powers, illustrating how grid Voltage stabilization is reached by the storage power response.

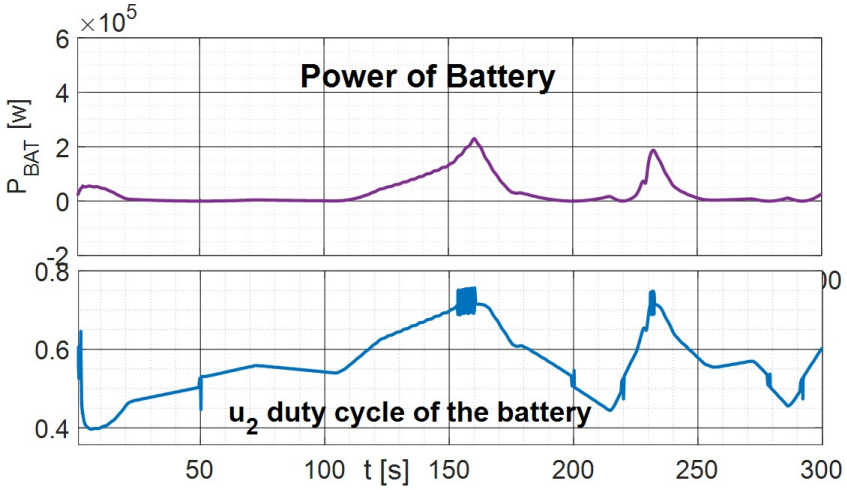

Figure 8. Control inputs u_2 and Output power of the battery.

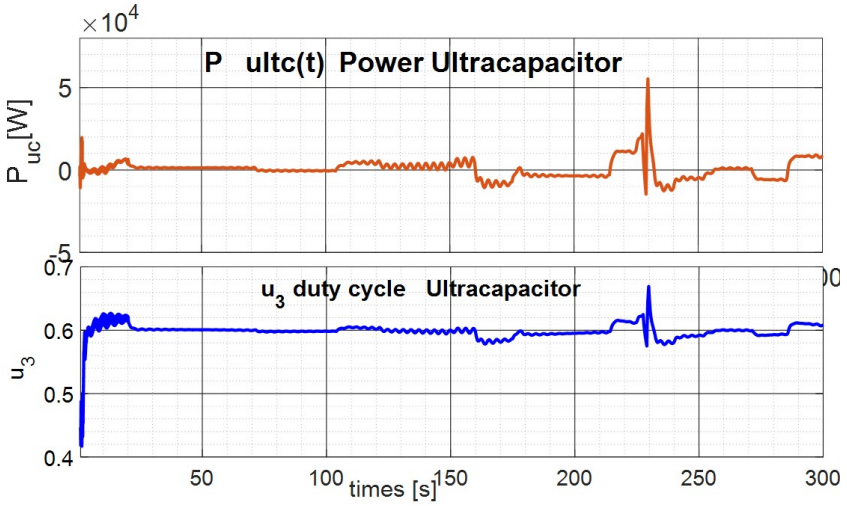

Figure 9. Control inputs u_3 and output power of the supercapacitor.

Figure 11 presents the DC voltage V_{DC} response for this longer simulation with slow power excursions. There, one may remark that the controller always keeps V_{DC} close to its nominal value despite these large power variations.

Figure 12 on the opposite, shows fast (step) load power variations. It can be seen how the DC bus voltage is kept stable inside its operation region, despite the fast variations on load and PV currents. The load current is equal to $576A$ for $5s < t < 42.8s$ and is equal to $138A$ elsewhere. The solar irradiance is kept at $1000W/m^2$ for $t < 12.4s$ and from $t > 24.8s$ it is set to $300W/m^2$. One can remark very small DC bus voltage variations following the transients, quickly recovering and stabilizing at the rated $(1000VDC)$ in about $10ms$. The maximum DC bus voltage error equals $4V = 0.4\%$, well inside the $\pm 5\%$ desired operation region.

The reference and actual waveforms for the battery are shown in the fourth screen from the top. Reference signal varies slowly for the battery resulting in very small errors. The reference and actual waveforms for the supercapacitor are shown in the fifth screen from the top. This reference varies much faster due to PV generation and load demand variations, returning to $0A$ after each transitory.

These results confirm that the proposed scheme is effective in achieving the goals defined for this application.

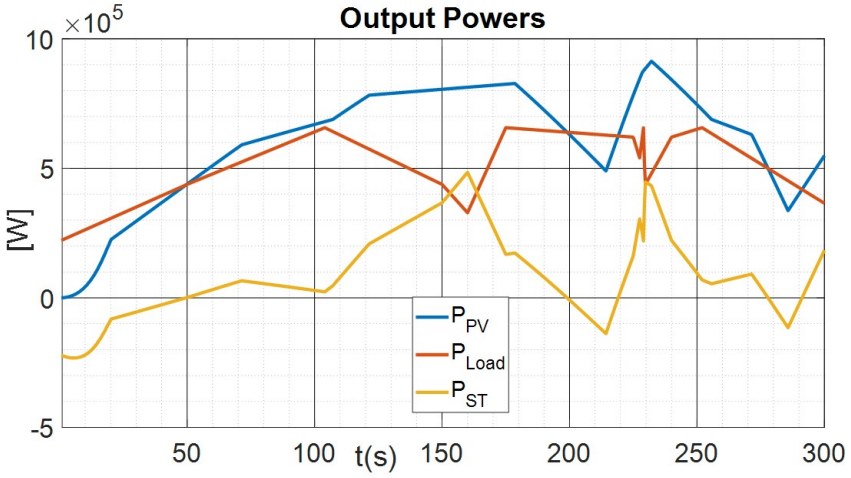

Figure 10. Output Power.

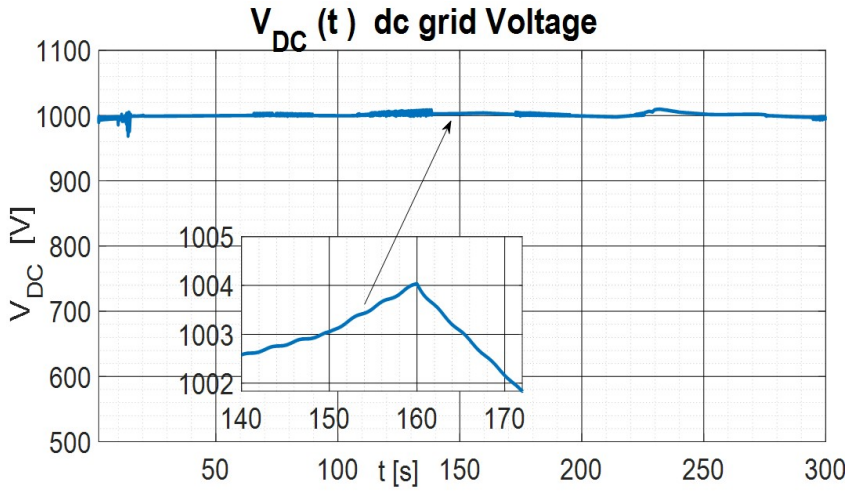

Figure 11. DC MicroGrid voltage.

5.1. Comparison with PI control

To illustrate the performance of the proposed controller, this one is compared to the industrial standard PI control. The global objective is to stabilize the DC voltage as fast as possible.

State space averaging method is used to obtain a Small Signal model for the converter ([45–47]). The model is formulated under the assumption that all the converter elements are ideal. The PI controllers are designed similarly to the ones presented in [48,49],[50],[51],[52]

In general the DC MicroGrid is connected to the main AC Grid and then $P_{DC} = P_{GRID}$, and balance power is supplied to or obtained from the AC Grid. In our work we will study the more difficult case when the DC MicroGrid is in islanded mode, and we can not rely on the AC network to balance the DC grid. In this case, any unbalance on power flow will create a voltage excursion on the DC grid.

From equation (6) we define the dynamic equation of voltage of DC MicroGrid :

$$\dot{V}_{DC} = \frac{1}{C_{DC}}[I_{PV} + I_{BR} + I_{ST} + I_{Load}] \tag{26}$$

The energy storage elements can switch between charge and discharge mode in order to maintain the DC grid power balance. $V_{DC}(t)$ must be kept around its nominal value and inside voltage limits following the power balance To present a performance comparison of the proposed controller, Figure 13 shows the results for the same simulation as above

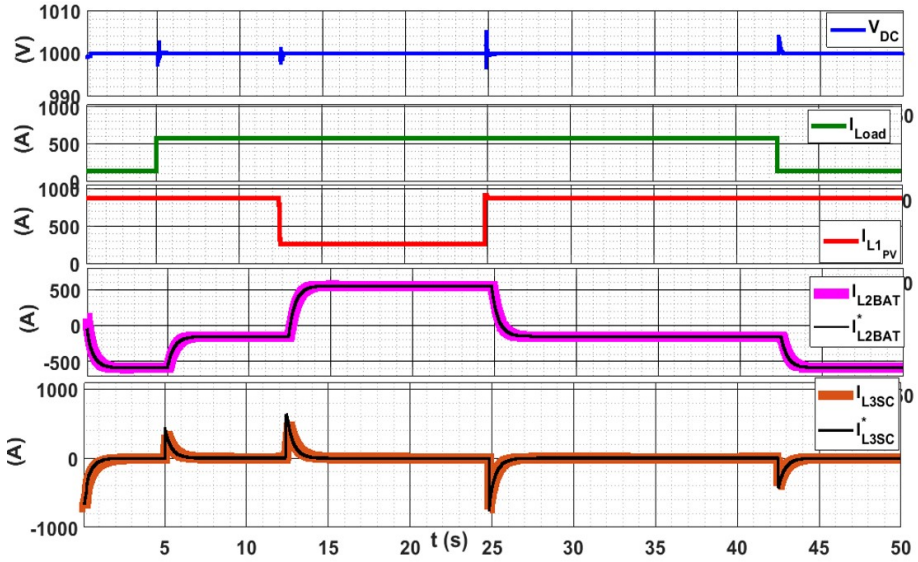

Figure 12. Dynamic response of the system.

using the industrial standard, a linear control (PI) for the DC MicroGrid voltage. The first picture of Figure 13 shows how the DC bus voltage (top) varies as the load current and PV current (following screens) vary. The load current is equal to $576A$ for $5s < t < 42.8s$ and is equal to $138A$ elsewhere. The solar irradiance was rated to $1000W/m^2$ for $t < 12.4s$ and $t > 24.8s$, and equal to $300W/m^2$ otherwise. There, one sees that the DC bus voltage varies briefly following the transients, recovering and stabilizing at the rated DC bus voltage of $1000VDC$ in about $1s$. The maximum DC bus voltage error is equal to $58V$.The battery's reference and actual waveforms are shown on the fourth screen from the top. The reference signal varies slowly and the actual waveform follows it with a small switching frequency ripple.

The supercapacitor's reference and actual waveforms are shown on the last screen from the top. The reference signal varies fast and the actual waveform follows it to cope with the generation and load variations, converging to $0A$ in steady state. One can also remark that the PI linear control response has bigger overshoots in transients and slower response.

Figure 14 presents a comparative study for the DC MicroGrid voltage. It can be seen that the DC bus voltage varies following each disturbance, recovering and stabilizing at the rated $(1000V)$. The maximum DC bus voltage error is equal to $55V$ for linear control in red. By using the PI linear control, the voltage V_{DC} oscillates during $1,2s$ before reaching steady state while the steady state response for the proposed nonlinear control is reached at $10ms$ as designed (it could be chosen to be faster though).

Steps	Peak overshoot Linear Control $V_{DC}[V]$	Peak overshoot Non Linear Control $V_{DC}[V]$	Settling time Linear Control $[s]$	Settling time Non Linear Control $[s]$
$t = 5s$	-58	-3	1.2	0.01
$t = 12.4s$	-45	-3	0.1	0.01
$t = 24.8s$	48	4	0.15	0.01
$t = 42.8s$	58	4	1	0.02

Table 2: Performance comparison with linear control and non linear control

Table (2) shows a comparison of voltage overshoot and settling time for several step changes in load demand and photovoltaic power. There one may remark that the

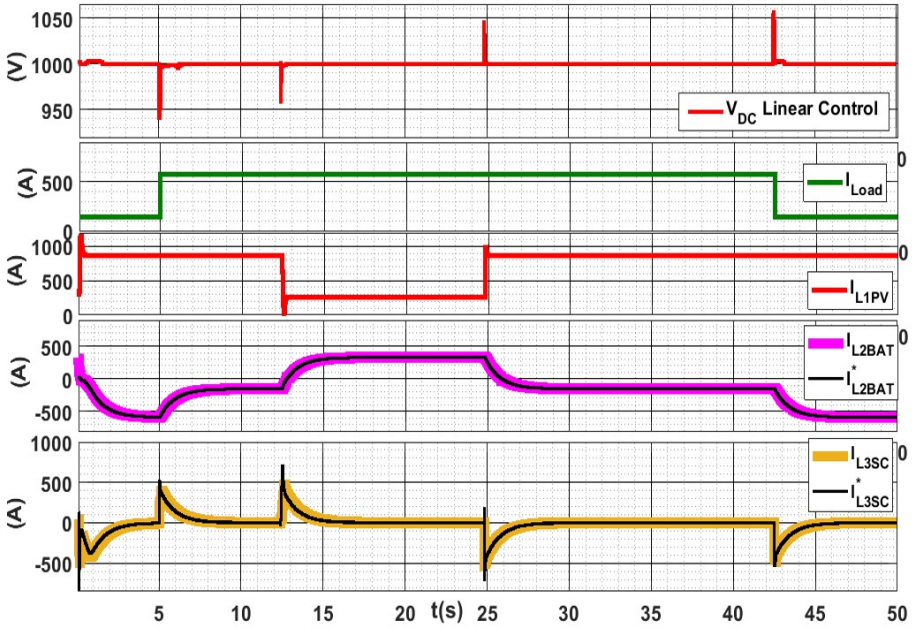

Figure 13. V_{DC} dynamics applying classical PI linear control.

nonlinear control has a much smaller overshoot (10%) than the linear PI. In the same way, settling time is much faster for the nonlinear control.

6. Conclusion

The efficient integration of distributed renewable power sources, especially fast intermittent sources as solar, is an essential but difficult task. It depends on developing flexible integration strategies to the network.

In this paper, a DC MicroGrid composed of PV panels and storage devices evolving in different time scales is considered to favor this integration, and controllers for each element are designed. A hierarchical control strategy is proposed such that it absorbs the maximum available renewable power while keeping the DC grid's voltage stable with respect to variations due to power production and consumption. The proposed control algorithm splits the power reference into fast and slow components, to be tracked by the supercapacitor and the battery respectively. As a consequence, the storage devices keep the DC voltage at the desired value and guarantee the balance between power generation and consumption. Moreover, in order to guarantee a suitable lifespan for the battery, the control strategy respects physical constraints.

Detailed simulation results corroborate our claims, and illustrate the good behavior of each element and the overall interconnected system. Compared to other results in the literature, this paper focuses on proposing easily implementable control algorithms, based on physical characteristics of the grid's elements, in order to obtain desired closed-loop dynamics and a formal stability proof. Future works will be dedicated to implementation in test-beds and the extension of the result to more complex meshed DC grids.

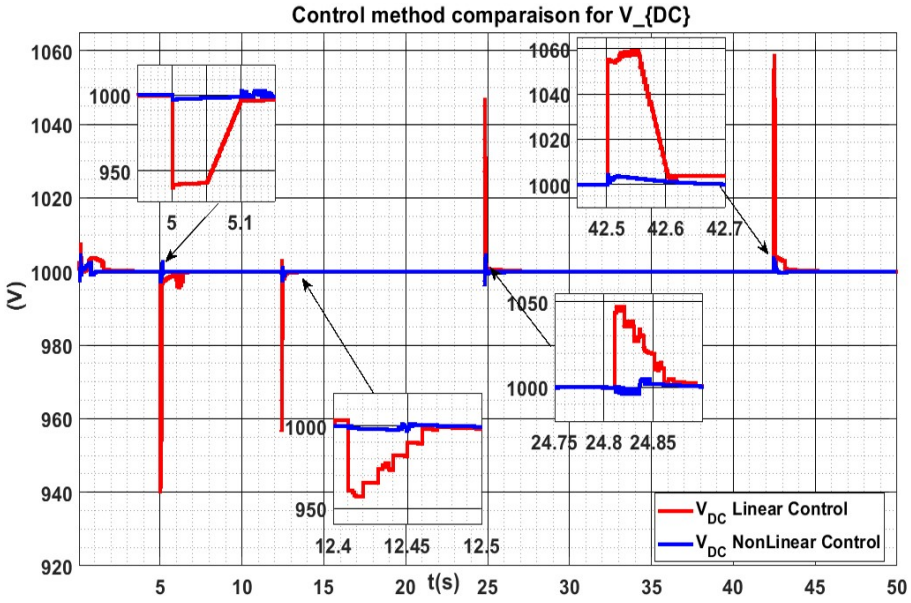

Figure 14. Comparison of the V_{DC} dynamics by applying nonlinear control (in blue) and classical PI control (in red).

I_{PV}	Output current of solar cell
P_{PV}	Output power of solar cell
V_{PV}	Terminal voltage of PV cell
I_{bat}	Output current of the battery
V_{bat}	Output voltage of the battery
P_{bat}	Output power of the battery
I_{sc}	Output current of the super capacitor
V_{sc}	Output voltage of the super capacitor
P_{sc}	Output power of the super capacitor
P_{DC}	Output power of the DC microgrid
T	Cell's reference Temperature
G	Solar irradiation
SOC	State of charge of battery
R_{01} ,R_{02}	internal resistances of DC/DC converter for the PV
R_1 ,R_2	resistances of DC/DC converter for the PV
L_1	inductance for the boost converter for the PV
C_1 C_2	capacitance of DC/DC converter for the PV
V_{C1} ,V_{C2}	Voltage of capacitance C_1 and $C_2$of DC/DC converter for the PV
i_{L1}	current of inductance L_1 for the boost converter for the PV
R_{03},R_{04}	internal resistances of DC/DC converter for the battery
R_3,R_4	resistances of DC/DC converter for the battery
L_2	inductance for the boost converter for the battery
C_3 C_4	capacitance of DC/DC converter for the battery
V_{C3} ,V_{C4}	Voltage of capacitance C_3 and $C_4$of DC/DC converter for the battery
i_{L2}	current of inductance L_1 for the boost converter for the battery
R_{05} ,R_{06}	internal resistances of DC/DC converter for the super capacitor
R_5 ,R_6	resistances of DC/DC converter for the super capacitor
L_3	inductance for the boost converter for the super capacitor
C_5 C_6	capacitance of DC/DC converter for the super capacitor
V_{C5} ,V_{C6}	Voltage of capacitance C_5 and $C_6$of DC/DC converter for the super capacitor
i_{L3}	current of inductance L_1 for the boost converter for the super capacitor
C_{dc}	DC-link capacitance of DC micro grid
f	Frequency of the AC grid
f_c	cutoff frequency for the filter
K_1..... K_{10}	positive tuning gains parameters
u_1, u_2 and u_3	Duties cycle of DC/DC converter

Table 3: List of Symbols

References

1. Hatziargyriou, N. *Microgrids: Architectures and Control*; John Wiley and Sons, 2014, 2014.
2. H.Bevrani.; Francois, B.; T.Ise. *Microgrid Dynamics and Control*; John Wiley and Sons Inc, 2017.
3. Ongaro, F.; Saggini, S.; Mattavelli, P. Li-Ion Battery-Supercapacitor Hybrid Storage System for a Long Lifetime, Photovoltaic-Based Wireless Sensor Network. *IEEE Transactions on Power Electronics* **2012**, *27*, 3944–3952.
4. Tahim, A.P.N.; Pagano, D.J.; Lenz, E.; Stramosk, V. Modeling and Stability Analysis of Islanded DC Microgrids Under Droop Control. *IEEE Transactions on Power Electronics* **2015**, *30*, 4597–4607.
5. Dulout, J.; Jammes, B.; Seguier, L.; Alonso, C. Control and design of a hybrid energy storage system. 2015 17th European Conference on Power Electronics and Applications (EPE 15 ECCE-Europe), 2015, pp. 1–9.
6. O Keeffe, D.; Riverso, S.; Albiol-Tendillo, L.; Lightbody, G. Distributed Hierarchical Droop Control of Boost Converters in DC Microgrids. 28th IEEE Irish Signals & Systems Conference, 2017.
7. Liang, C.; Zhang, Y.; Ji, X.; Meng, X.; An, Y.; Yao, Q. DC Bus Voltage Sliding-mode Control for a DC Microgrid Based on Linearized Feedback. 2019 Chinese Automation Congress (CAC), 2019, pp. 5380–5384. doi:10.1109/CAC48633.2019.8996266.
8. Kollimalla, S.K.; Mishra, M.K.; Narasamma, N.L. Design and Analysis of Novel Control Strategy for Battery and Supercapacitor Storage System. *IEEE Transactions on Sustainable Energy* **2014**, *5*, 1137–1144.
9. Ferreira, R.A.F.; Barbosa, P.G.; Braga, H.A.; Ferreira, A.A. Analysis of non-linear adaptive voltage droop control method applied to a grid connected DC microgrid. 2013 Brazilian Power Electronics Conference, 2013, pp. 1067–1074. doi:10.1109/COBEP.2013.6785247.
10. Chen, Y.; Damm, G.; Benchaib, A.; Netto, M.; Lamnabhi-Lagarrigue, F. Control Induced Explicit Time-Scale Separation to Attain DC Voltage Stability for a VSC-HVDC Terminal. *IFAC Proceedings Volumes* **2014**, *47*, 540 – 545. 19th IFAC World Congress.
11. Iovine, A.; Siad, S.B.; Damm, G.; De Santis, E.; Di Benedetto, M.D. Nonlinear Control of a DC MicroGrid for the Integration of Photovoltaic Panels. *IEEE Transactions on Automation Science and Engineering* **2017**, *14*, 524–535. doi:10.1109/TASE.2017.2662742.
12. Siad, S.B.; Malkawi, A.; Damm, G.; Lopes, L.; Dol, L.G. Nonlinear control of a DC MicroGrid for the integration of distributed generation based on different time scales. *International Journal of Electrical Power and Energy Systems* **2019**, *111*, 93–100. doi:https://doi.org/10.1016/j.ijepes.2019.03.073.
13. Siad, S.; Damm, G.; Dol, L.G.; Bernardinis, A.d. Design and Control of a DC Grid for Railway Stations. PCIM Europe 2017; International Exhibition and Conference for Power Electronics, Intelligent Motion, Renewable Energy and Energy Management, 2017, pp. 1–8.
14. Guerrero, J.M.; Loh, P.C.; Lee, T.; Chandorkar, M. Advanced Control Architectures for Intelligent Microgrids—Part II: Power Quality, Energy Storage, and AC/DC Microgrids. *IEEE Transactions on Industrial Electronics* **2013**, *60*, 1263–1270.
15. Carrizosa, M.J.; Navas, F.D.; Damm, G.; Lamnabhi-Lagarrigue, F. Optimal power flow in multi-terminal HVDC grids with offshore wind farms and storage devices. *International Journal of Electrical Power & Energy Systems* **2015**, *65*, 291 – 298.
16. Carrizosa, M.J.; Arzandé, A.; Navas, F.D.; Damm, G.; Vannier, J. A control strategy for multi-terminal DC grids with renewable production and storage devices. *IEEE Transactions on Sustainable Energy* **2018**, *9 NO 2*.
17. Siad, S. DC MicroGrids Control for Renewable Energy Integration. PhD thesis, University Evry, 2019.
18. Iovine, A.; Siad, S.; Damm, G.; De Santis, E.; Di Benedetto, M.D. Nonlinear Control of an AC-connected DC MicroGrid. 42nd Annual Conference of the IEEE Industrial Electronics Society - IECON 2016, 2016.
19. Iovine, A.; Carrizosa, M.J.; Damm, G.; Alou, P. Nonlinear Control for DC MicroGrids enabling Efficient Renewable Power Integration and Ancillary Services for AC grids. *IEEE Transactions on Power Systems* **2019**, *to appear*.
20. Iovine, A.; Rigaut, T.; Damm, G.; De Santis, E.; Di Benedetto, M.D. Power management for a DC MicroGrid integrating renewables and storages. *Control Engineering Practice* **2019**, *85*, 59 – 79. doi:https://doi.org/10.1016/j.conengprac.2019.01.009.
21. Benchaib, A. *Advanced Control of AC / DC Power Networks: System of Systems Approach Based on Spatio-temporal Scales*; Wiley-ISTE, 2015.
22. Lee, J.; Han, B.; Choi, N. DC micro-grid operational analysis with detailed simulation model for distributed generation. 2010 IEEE Energy Conversion Congress and Exposition, 2010, pp. 3153–3160.
23. G.Krajacic.; Duic, N.; B.V.Mathiesen.; Carvalho, M.G. Smart energy storages for integration of renewable in 100 % independent energy systems. *Chemical Engineering Transactions* **2010**, *21*, 391–396.
24. Yahya, A.M.; Mahmoud, A.; L.Youm. Etude et modellisation d'un generateur photovoltaique. *Revue des Energies Renouvelables* **2008**, *11*, 473–483.
25. Sera, D.; Teodorescu, R.; Hantschel, J.; Knoll, M. Optimized Maximum Power Point Tracker for fast changing environmental conditions. 2008 IEEE International Symposium on Industrial Electronics, 2008, pp. 2401–2407.
26. Xiao, W. A modified adaptive hill climbing maximum power point tracking (MPPT) control method for photovoltaic power systems. PhD thesis, Vancouver : University of British Columbia Library, 2003.
27. S.Bacha.; I.Munteanu.; A.I.Bratcu. *Power Electronic Converters Modeling and Control: with Case Studies*; Advanced Textbooks in Control and Signal Processing, Springer London, 2013.
28. Merdassi, A.; Gerbaud, L.; Seddik, B. General Average Modelling for Power Electronics Systems: Automatic Building Approach. Conference: Conference: 9th International Conference on Modeling and Simulation of Electric Machines, Converters and Systems, At Quebec, Canada, 2008.
29. Merdassi.A. *La modellisation Automatique pour l'electronique de puissance*; Editions Universitaires Europeennes, 2010.

30. Sanders, S.R.; Noworolski, J.M.; Liu, X.Z.; Verghese, G.C. Generalized averaging method for power conversion circuits. *IEEE Transactions on Power Electronics* **1991**, *6*, 251–259.
31. J.Barton.; Infield, D. Energy storage and its use with intermittent renewable energy. *EEE Transactions on Energy Conversion* **2004**, *19*, 441–448.
32. Bhatia, R.S.; Singh, B.; Jain, D.K.; Jain, S.P. Battery Energy Storage System Based Power Conditioner for Improved Performance of Hybrid Power Generation. 2008 Joint International Conference on Power System Technology and IEEE Power India Conference, 2008, pp. 1–6.
33. O.Gergaud.; G.Robin.; B.Multon.; AHMED, H. Energy Modeling of a Lead-Acid Battery within Hybrid Wind/Photovoltaic Systems. European Power Electronic Conference 2003; , 2003; p. 8pp.
34. VAIRAMOHAN.B. State of charge estimation for batteries. Master's thesis, University of Tennessee, Knoxville, 2002.
35. *Miller JM., Nebrigic. D, Everett.M Ultra capacitor Distributed Model Equivalent Circuit for Power Electronic Circuit Simulation. Maxwell Technologies Inc. San diego. CA. Ansoft Leading Insights Workshop. July 2006.*
36. D.Lifshitz.; Weiss.G. Optimal control of a capacitor-type energy storage system,. *Automatic Control, IEEE Transactions* **2015**, *vol. 60*, pp. 216?220.
37. Odo, P. A Comparative Study of Single-phase Non-isolated Bidirectional dc-dc Converters Suitability for Energy Storage Application in a dc Microgrid **2020**. pp. 391–396. doi:10.1109/PEDG48541.2020.9244351.
38. Sun, J.; Lin, W.; Hong, M.; Loparo, K.A. Voltage Regulation of DC-Microgrid With PV and Battery. *IEEE Transactions on Smart Grid* **2020**, *11*, 4662–4675. doi:10.1109/TSG.2020.3005415.
39. Adhikari, S.; Li, F. Coordinated V-f and P-Q Control of Solar Photovoltaic Generators With MPPT and Battery Storage in Microgrids. *IEEE Transactions on Smart Grid* **2014**, *5*, 1270–1281.
40. Manandhar, U.; Ukil, A.; Gooi, H.B.; Tummuru, N.R.; Kollimalla, S.K.; Wang, B.; Chaudhari, K. Energy Management and Control for Grid Connected Hybrid Energy Storage System Under Different Operating Modes. *IEEE Transactions on Smart Grid* **2019**, *10*, 1626–1636. doi:10.1109/TSG.2017.2773643.
41. Chen, Y.; Jiménez Carrizosa, M.; Damm, G.; Lamnabhi-Lagarrigue, F.; Li, M.; Li, Y. Control-Induced Time-Scale Separation for Multiterminal High-Voltage Direct Current Systems Using Droop Control. *IEEE Transactions on Control Systems Technology* **2019**, pp. 1–17. doi:10.1109/TCST.2019.2901343.
42. Fei, Y.; Zhuang, J.; Li, G.; Yao, L.; Yang, B. Research on the dual-terminal ring topology-based dc microgrid system. *The Journal of Engineering* **2018**, *2019*. doi:10.1049/joe.2018.8764.
43. Kumar, D.; Zare, F.; Ghosh, A. DC Microgrid Technology: System Architectures, AC Grid Interfaces, Grounding Schemes, Power Quality, Communication Networks, Applications, and Standardizations Aspects. *IEEE Access* **2017**, *5*, 12230–12256. doi:10.1109/ACCESS.2017.2705914.
44. Khalil, H. *Nonlinear Systems*; Pearson; Edition, 2002.
45. Jin, Y.; Xu, J.; Zhou, G.; Mi, C. Small-signal modeling and analysis of improved digital peak current control of boost converter. 2009 IEEE 6th International Power Electronics and Motion Control Conference, 2009, pp. 326–330.
46. Tang, W.; Lee, F.C.; Ridley, R.B. Small-signal modeling of average current-mode control. *IEEE Transactions on Power Electronics* **1993**, *8*, 112–119.
47. Sun, J.; Bass, R.M. Modeling and practical design issues for average current control. APEC '99. Fourteenth Annual Applied Power Electronics Conference and Exposition. 1999 Conference Proceedings, 1999, Vol. 2, pp. 980–986.
48. Cherati, S.M.; Azli, N.A.; Ayob, S.M.; Mortezaei, A. Design of a current mode PI controller for a single-phase PWM inverter. 2011 IEEE Applied Power Electronics Colloquium (IAPEC), 2011, pp. 180–184.
49. *L. H. Dixon, Average Current Mode Control of Switching Power Supplies,Unitrode Power Supply Design Seminar Manual, 1990.*
50. Khalid, M. A Review on the Selected Applications of Battery-Supercapacitor Hybrid Energy Storage Systems for Microgrids. *Energies* **2019**, *12*, 4559. doi:10.3390/en12234559.
51. Kollimalla, S.K.; Mishra, M.K.; Ukil, A.; Gooi, H.B. DC Grid Voltage Regulation Using New HESS Control Strategy. *IEEE Transactions on Sustainable Energy* **2017**, *8*, 772–781. doi:10.1109/TSTE.2016.2619759.
52. Manandhar, U.; Tummuru, N.R.; Kollimalla, S.K.; Ukil, A.; Beng, G.H.; Chaudhari, K. Validation of Faster Joint Control Strategy for Battery- and Supercapacitor-Based Energy Storage System. *IEEE Transactions on Industrial Electronics* **2018**, *65*, 3286–3295. doi:10.1109/TIE.2017.2750622.